Nanostructured Materials and Functional Coatings
Наноструктурированные материалы и функциональные покрытия

UDC 621.762
https://doi.org/10.17073/1997-308X-2025-2-62-72

*Research article*
*Научная статья*



# Use of Ni and Al granules and WC powder for electric spark deposition of metalloceramic coatings

**A. A. Burkov**

**Khabarovsk Federal Research Center**
**of the Far Eastern Branch of the Russian Academy of Sciences**
153 Tikhookeanskaya Str., Khabarovsk 680042, Russia

burkovalex@mail.ru

***Abstract.*** Research on novel metalloceramic coatings that combine high-temperature oxidation resistance and wear resistance remains a relevant topic. Ni–Al–Fe coatings reinforced with varying amounts of tungsten carbide were synthesized for the first time using electric spark deposition on 35 steel. Their structure was analyzed using *X*-ray phase analysis and scanning electron microscopy. The average thickness of the WC/Ni–Al–Fe coatings ranged from 23 to 33 μm. The identified phases included AlNi, (Fe, Ni), α-WC, and $W_2C$. The coating microstructure exhibited reinforcing tungsten carbide inclusions with diameters ranging from 1.49 to 10.12 μm. The corrosion behavior of coated samples was studied using potentiodynamic polarization and impedance spectroscopy in a 3.5 % NaCl solution. The coatings' high-temperature oxidation resistance was evaluated at 700 °C for 110 h under natural aeration conditions. Wear testing was conducted under dry friction conditions at loads of 25 and 50 N. The results demonstrate that the application of WC/Ni–Al–Fe-coatings can reduce the specific wear of the steel surface by a factor of 11 to 24 and enhances resistance to high-temperature oxidation by a factor of 10.5 to 49.9.

***Keywords:*** WC/Ni–Al–Fe coatings, electric spark deposition, nonlocalized electrode (NLE), St3 steel, *X*-ray phase analysis, corrosion, friction coefficient, hardness, wear

***Acknowledgements:*** The work was carried out within the framework of state assignment No. 075-01108-23-02.

***For citation:*** Burkov A.A. Use of Ni and Al granules and WC powder for electric spark deposition of metalloceramic coatings. *Powder Metallurgy and Functional Coatings*. 2025;19(2):62–72. https://doi.org/10.17073/1997-308X-2025-2-62-72

# Использование гранул Ni и Al и порошка WC для электроискрового нанесения металлокерамических покрытий

**А. А. Бурков**

**Хабаровский федеральный исследовательский центр**
**Дальневосточного отделения Российской академии наук**
Россия, 680042, г. Хабаровск, ул. Тихоокеанская, 153

burkovalex@mail.ru

***Аннотация.*** Исследования новых металлокерамических покрытий, сочетающих высокую жаростойкость и устойчивость к износу, являются актуальными. Ni–Al–Fe покрытия, армированные различным количеством карбида вольфрама, впервые получены методом электроискрового легирования на стали 35. Их структура исследовалась методами рентгеноструктурного фазового анализа и сканирующей электронной микроскопии. Средняя толщина WC/Ni–Al–Fe-покрытий составляла от 23 до 33 мкм. В их составе идентифицированы фазы AlNi, (Fe, Ni), α-WC и $W_2C$. В микроструктуре покрытий наблюдались армирующие включения карбида вольфрама диаметром от 1,49 до 10,12 мкм. Коррозионное поведение образцов

с покрытиями изучалось методами потенциодинамической поляризации и импедансной спектроскопии в 3,5 %-ном растворе NaCl. Жаростойкость покрытий исследовалась при температуре 700 °C в течение 110 ч в условиях естественной аэрации. Тестирование на износ проводилось в режиме сухого трения при нагрузках 25 и 50 Н. Показано, что применение WC/Ni–Al–Fe-покрытий позволяет сократить приведенный износ поверхности стальных изделий с 11 до 24 раз и повысить стойкость к высокотемпературной газовой коррозии с 10,5 до 49,9 раза.

***Ключевые слова:*** покрытия WC/Ni–Al–Fe, электроискровое легирование, нелокализованный электрод (НЭ), сталь Ст3, рентгенофазовый анализ, коррозия, коэффициент трения, твердость, износ

***Благодарности:*** Работа выполнена в рамках государственного задания № 075-01108-23-02.

***Для цитирования:*** Бурков А.А. Использование гранул Ni и Al и порошка WC для электроискрового нанесения металлокерамических покрытий. *Известия вузов. Порошковая металлургия и функциональные покрытия*. 2025;19(2):62–72. https://doi.org/10.17073/1997-308X-2025-2-62-72

## Introduction

Metalloceramic composites (MCCs) are among the most widely used wear-resistant materials [1]. They typically consist of hard carbide particles (WC, TiC, $TiB_2$, TaC, NbC) bonded by ductile metallic phases such as Co, Fe, and Ni [2]. The carbide particles in these composites provide high hardness and wear resistance, while the binder phase enhances toughness. Over the past century, among various carbide-based materials, tungsten carbide (WC) composites have found the broadest application across multiple industries [3–5]. A key aspect of this class of metalloceramics is the type of metallic binder used.

For many years, cobalt has been the most commonly used metallic binder due to its excellent wettability with tungsten carbide grains and the high impact toughness it provides [6]. However, its use raises serious environmental concerns and is further limited by its high cost. Studies indicate that prolonged inhalation exposure to cobalt can cause allergic reactions and cancer [7]. Additionally, its poor corrosion and oxidation resistance, along with unsatisfactory mechanical performance at temperatures above 600 °C, have driven researchers to seek alternative binders [8].

For instance, intermetallic Ni–Al alloys are sometimes considered as metallic binders [9; 10] due to their favorable properties, including high melting points, heat resistance, low density, and excellent oxidation resistance, which can compensate for tungsten carbide's poor oxidation resistance [11].

Iron aluminide (FeAl) is known to be a suitable binding matrix for tungsten carbide due to its favorable properties, including good wettability with WC, enhanced hardness, low density, and high oxidation resistance in oxidative, carburizing, and sulfidizing environments [12]. A dense $Al_2O_3$ film, known for its excellent protective properties, can form on the surface of nickel and iron aluminides [13]. However, ternary Al–Ni–Fe alloys remain significantly less studied [14], despite their potential for enhanced hardness and oxidation resistance, while also requiring less nickel compared to NiAl-based materials. Additionally, nickel alloying of FeAl has been shown to induce significant solid-solution strengthening [15].

Tungsten carbide-based metalloceramic composites are widely used as coatings on structural metals to improve hardness, wear resistance, and oxidation resistance [16; 17]. For instance, in studies [18; 19], WC/FeAl coatings were deposited onto structural steels using laser cladding and high-velocity arc spraying. However, tungsten carbide-based coatings with Ni–Al and Ni–Al–Fe matrices have been explored to a much lesser extent. In [20], WC/NiAl/TiC coatings were prepared using laser cladding. A $(NiAl)_{0.8}WC_{0.2}$–Fe(0–15 wt. %) coating with a ternary Ni–Al–Fe matrix was deposited onto low-alloy Q235 steel using plasma cladding [17].

The electric spark deposition (ESD) method is employed for depositing metallic and metalloceramic materials onto metal substrates and is characterized by minimal thermal impact on the base material's structure, while producing coatings with strong adhesion [21]. The use of a nonlocalized electrode (NLE) in ESD enables automation of the deposition process, including applications on complex-shaped components [22]. In our previous study, the electric spark deposition with a nonlocalized electrode (ESD-NLE) method was used to produce WC/Fe–Al coatings, where the NLE consisted of aluminum and iron granules combined with α-WC powder [23].

The objective of this study is to investigate the feasibility of producing metalloceramic coatings using the ESD-NLE method on 35 steel, using Ni and Al granules along with WC powder.

## Materials and methods

The composition of the NLE is shown in Table 1. The aluminum alloy 1188 and high-purity nickel (99.99 %) granules were shaped as cylinders ($h = 4 \pm 1$ mm, $d = 4 \pm 0.5$ mm) and cubes

***Table 1.*** **Coating designation based on NLE composition**

***Таблица 1.*** **Маркировка покрытий в зависимости от состава НЭ**

| Sample | Granule ratio, at. % | | Granule fraction, vol. % | WC powder fraction, vol. % |
|---|---|---|---|---|
| | Al | Ni | | |
| ANW2 | 15 | 85 | 98 | 2 |
| ANW4 | | | 96 | 4 |
| ANW6 | | | 94 | 6 |

(4×4×4 ± 0.5 mm), respectively. The tungsten carbide powder (TU 6-09-03-360-78) had a purity of 99.9 % and an average particle diameter of 1.1 ± 0.3 μm. The NLE composition was designed with a dominance of nickel, maintaining a Ni/Al ratio of 17:3, as aluminum has significantly lower electroerosion resistance than nickel [24]. The 35 steel substrate acted as an iron source for the WC/Ni–Al–Fe coatings, as iron from the steel base is known to diffuse into ESD coatings [23]. Fig. 1 illustrates the schematic of the ESD setup operating in an environment of granules and powder.

The 35 steel substrate was fabricated in the form of a cylinder ($d$ = 12 mm, $h$ = 10 mm). The IMES-40 power generator, operating at 30 V, produced current pulses with an amplitude of 110 A, a duration of 100 μs, and a period of 1000 μs. To minimize oxidation, coating deposition was carried out under an argon flow (5 L/min). The deposition time for each sample was 10 min.

The phase composition of the obtained coatings was analyzed using a DROH-7 $X$-ray diffractometer (NPP Burevestnik, Russia) with Cu$K_\alpha$ radiation (λ = 1.54056 Å). The microstructure and elemental composition of the coatings were examined using a Vega 3 LMH scanning electron microscope (Tescan, Czech Republic) equipped with an X-max 80 energy-dispersive spectrometer (EDS) (Oxford Instruments, UK). The surface roughness of the coatings was measured using the $R_a$ parameter with a Profilometer 296 (USSR). The wettability of the coated surfaces with deionized water was evaluated using the sessile drop method at 25 °C [25]. The Vickers hardness of the coatings was measured using a PMT-3M microhardness tester under a 1.96 N load. Tribological tests were conducted following the ASTM G99-17 procedure using the pin-on-disk configuration (without rounding of the pin end) at a rotation frequency of 3 rev/s under loads of 25 and 50 N for 10 min. High-speed steel M45 disks ($d$ = 50 mm, 60 HRC) were used as counterbodies.

The tribological tests were performed on a laboratory test bench equipped with a M40-50 non-contact torque sensor (Belarus). The specific wear rate was determined gravimetrically, considering the density of the coatings, which was calculated using the rule of mixtures based on the chemical composition. The electrochemical corrosion tests of coated samples were conducted using a P-40X potentiostat-galvanostat (Electro Chemical Instruments, Russia) equipped with an impedance measurement module, in a standard

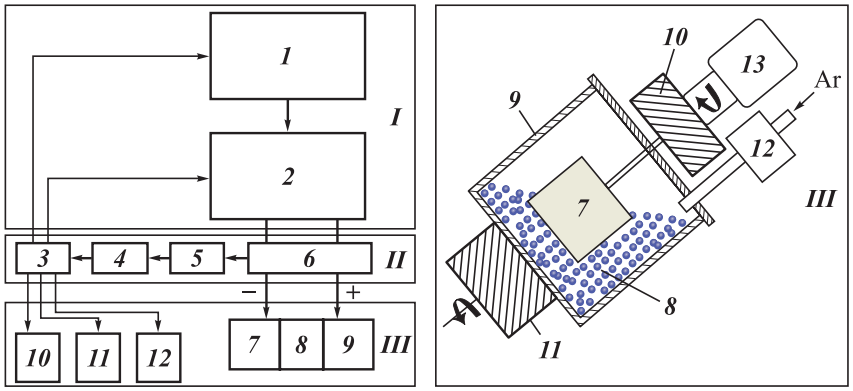


***Fig. 1.*** Schematic of the experimental setup for electric spark granules deposition of granules

***I*** – pulse discharge generation unit, ***II*** – measuring and control unit, ***III*** – electrode switching unit
***1*** – control pulse generator, ***2*** – power generator, ***3*** – microcontroller, ***4*** – computer, ***5*** – analog-to-digital converter,
***6*** – current and voltage measuring device, ***7*** – cathode (35 steel), ***8*** – Ni and Al granules, WC powder, ***9*** – current lead (container),
***10***, ***11*** – motors for the cathode and the granule container, respectively, ***12*** – gas solenoid valve, ***13*** – micromanipulator

***Рис. 1.*** Схема экспериментальной установки для электроискрового осаждения гранул

***I*** – блок генерации разрядных импульсов, ***II*** – измерительный и управляющий блок,
***III*** – блок коммутации электродов
***1*** – генератор управляющих импульсов, ***2*** – силовой генератор, ***3*** – микроконтроллер, ***4*** – компьютер,
***5*** – аналого-цифровой преобразователь, ***6*** – измерительное устройство тока и напряжения, ***7*** – катод (сталь 35),
***8*** – гранулы Ni и Al, порошок WC, ***9*** – токопровод (контейнер), ***10***, ***11*** – двигатели катода и контейнера с гранулами соответственно,
***12*** – газовый электроклапан, ***13*** – микроманипулятор

three-electrode cell containing a 3.5 % NaCl solution. An Ag/AgCl electrode served as the reference electrode, while an ETP-02 platinum electrode was used as the counter electrode. To stabilize the open-circuit potential, the samples were immersed in the electrolyte solution for 60 min before measurements.

Cyclic oxidation resistance was tested at 700 °C. The samples were placed in a preheated muffle furnace, held for approximately 6 h, then transferred to a desiccator until fully cooled before weighing. During testing, the samples were kept in corundum crucibles to prevent the loss of spalled oxide scale. The total test duration was 100 h.

## Results and discussion

When testing new electrode materials, it is essential to record mass transfer during ESD to determine the specific mass gain of the cathode, as this parameter defines the thickness of the formed coating [21]. As the number of discharge pulses increased (i.e., with longer ESD-NLE duration), the cathode continuously gained mass (Fig. 2). Over 10 min of ESD-NLE, the total specific mass gain ranged from 4.2 to 6.3 mg/cm$^2$. The average values were independent of the electrode type, considering the measurement error.

Fig. 3, *a*, *c*, and *e* show cross-sections of WC/Ni–Al–Fe coatings. As seen from Table 2, their average thickness is practically independent of the WC powder content in the NLE, ranging from 31.5 to 32.7 μm. The coating structure consists of a gray matrix reinforced with bright inclusions of micron- and submicron-sized particles. The diameter of the micron-sized inclusions ranges from 3 to 20 μm, and these are agglomerates of the original WC powder particles. According to EDS data, as the WC powder content in the NLE increases, the coating matrix composition is monotonically enriched with tungsten and iron, while the nickel and aluminum concentrations decrease (Fig. 3, *b*, *d*, *f*).

As the WC content in the NLE increases from ANW2 to ANW6, the average tungsten concentration in the coating matrix rises from 5.3 to 23.2 at. %, while the iron content increases from 35.5 to 57.6 at. %, and the nickel concentration decreases from 35.3 to 4.8 at. %. This is due to the fact that the powder elements in the ESD-NLE coating are present in disproportionately higher amounts than the granule components, a trend we previously observed [26]. ANW2 coating has the most balanced atomic ratio of aluminum, nickel, and iron.

Thus, adjusting the WC powder fraction in the electrode enables control over the metal ratio in the coating. The high iron concentration in the ANW6 coating matrix confirms the substrate material's involvement in the formation of the ESD coating. As the WC powder fraction in the NLE increases, the proportion of white inclusions in the coatings also rises, as seen in Fig. 3, *a*, *c*, *e*.

A small number of transverse microcracks are present in the coatings. These form due to rapid cooling of the material after discharge, caused by the difference in the coefficients of linear thermal expansion between the coating and the substrate [27]. The absence of longitudinal cracks and the gradual change in metal concentrations at the coating-substrate interface indicate strong adhesion of the WC/Ni–Al–Fe coatings to 35 steel. The coating roughness ($R_a$) ranged from 4.5

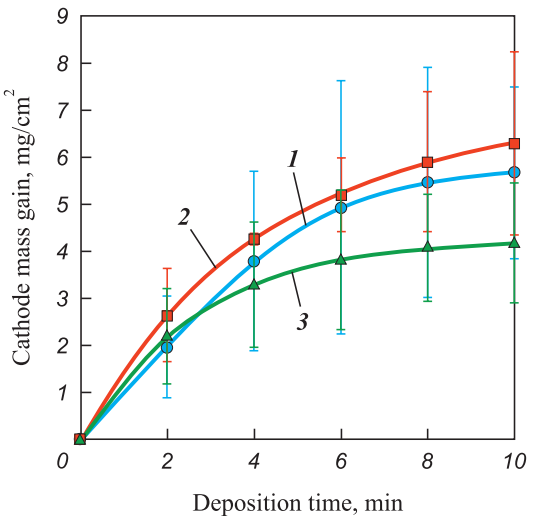


***Fig. 2.*** Dependence of cathode mass gain on ESD-NLE duration
***1*** – ANW2, ***2*** – ANW4, ***3*** – ANW6

***Рис. 2.*** Зависимость привеса катода от продолжительности ЭИЛНЭ
***1*** – ANW2, ***2*** – ANW4, ***3*** – ANW6

***Table 2.*** **Characteristics of WC/Ni–Al–Fe coatings**

***Таблица 2.*** **Характеристики WC/Ni–Al–Fe-покрытий**

| Characteristic | ANW2 | ANW4 | ANW6 |
|---|---|---|---|
| Thickness, μm | 32.42 ± 1.77 | 31.48 ± 6.93 | 32.66 ± 2.48 |
| Roughness, μm | 4.50 ± 0.90 | 4.77 ± 1.10 | 4.51 ± 0.80 |
| Wettability, deg | 80.0 | 82.1 | 81.9 |

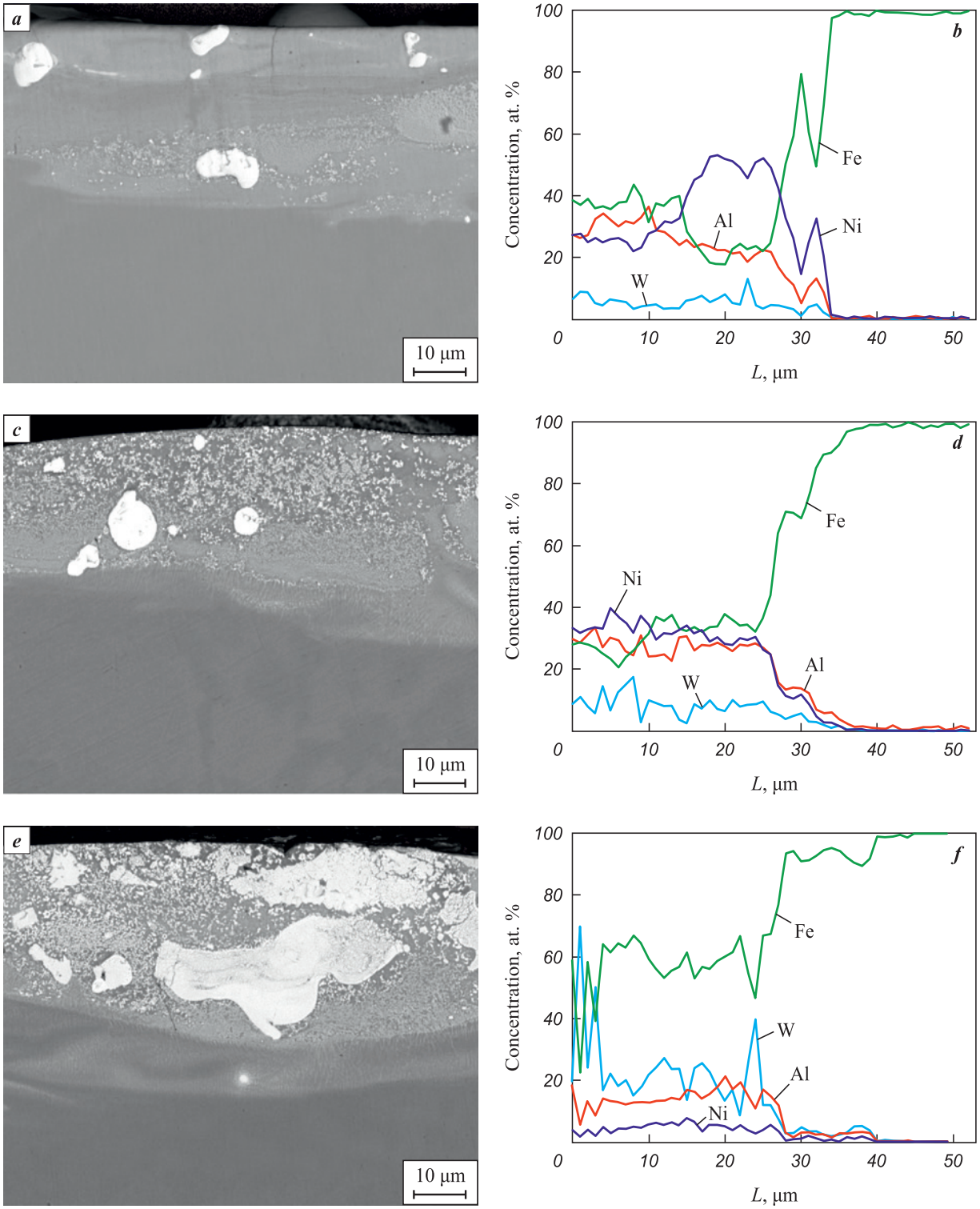


***Fig. 3.*** SEM images and elemental distribution in the cross-section of ANW2 (***a***, ***b***), ANW4 (***c***, ***d***), and ANW6 (***e***, ***f***) coatings

***Рис. 3.*** СЭМ-изображения и распределение элементов в поперечном сечении покрытий ANW2 (***a***, ***b***), ANW4 (***c***, ***d***) и ANW6 (***e***, ***f***)

to 4.77 μm and did not depend on the WC powder concentration (see Table 2). The contact angle of the coating surface with distilled water was between 80.0 and 82.1°, significantly higher than that of 35 steel (65.9°). Thus, the application of WC/Ni–Al–Fe coatings imparts hydrophobic properties to the steel surface.

According to Fig. 4, *a*, *c*, the large inclusions correspond to grains of the initial tungsten carbide (α-WC). Submicron inclusions formed after the discharge ceased, during the solidification of the Fe–W–Ni–Al–C melt (Fig. 4, *b*). A similar microstructure was previously observed in ESD coatings

on 35 steel deposited using WC–Co anodes [28]. Thus, the formation of WC/Ni–Al–Fe coatings via ESD proceeds through two stages: sintering of refractory agglomerated WC particles and eutectic crystallization of the Fe–W–Ni–Al–C melt [29].

The results of *X*-ray phase analysis of the WC/Ni–Al–Fe coatings are shown in Fig. 5. The data indicate that, in addition to WC and $W_2C$, the coatings contain the intermetallic compound AlNi (PDF card #44-1188 from the PdWin database) and a face-centered cubic (FCC) Fe–Ni solid solution [30], which serve as the metallic matrix. The presence of ferro-nickel is attributed to the high nickel concentration in the ANW2 coating (see Fig. 2, *b*). The α-WC carbide and $W_2C$ subcarbide act as reinforcing phases in the metalloceramic coating. The formation of $W_2C$ occurs due to the decarburization of WC when it interacts with the iron melt in the micro-melt pool under electric discharge temperatures [24]. This is supported by an increase in the $W_2C$ content from 14.1 to 24.1 vol. % (Table 3) as the iron concentration rises from ANW2 to ANW6 (see Figs. 3, *b*, *d*, *f*). Fig. 4, *a* illustrates the interaction between a tungsten carbide particle and the iron melt.

The WC phase fraction in the coatings increased from 48.6 to 65.5 vol. % with the addition of tungsten carbide powder to the NLE, while the intermetallic fraction decreased from 28.2 to 10.3 vol. %. Notably, such a high WC content in the coatings cannot be achieved using conventional single-electrode ESD on steels with hardmetal anodes, due to the high solubility of WC in liquid iron [31].

Based on the coating microstructure, the formation of mechanism of WC/Ni–Al–Fe coating during ESD-NLE can be described as follows: when a Ni or Al granule comes into electrical contact with the substrate, low-voltage discharges occur, causing the transfer of molten granule material into the micro-melt pool on the cathode surface. Tungsten carbide powder particles, located on the electrode surface within the discharge initiation and propagation zone, become wetted by metal droplets and are incorporated into

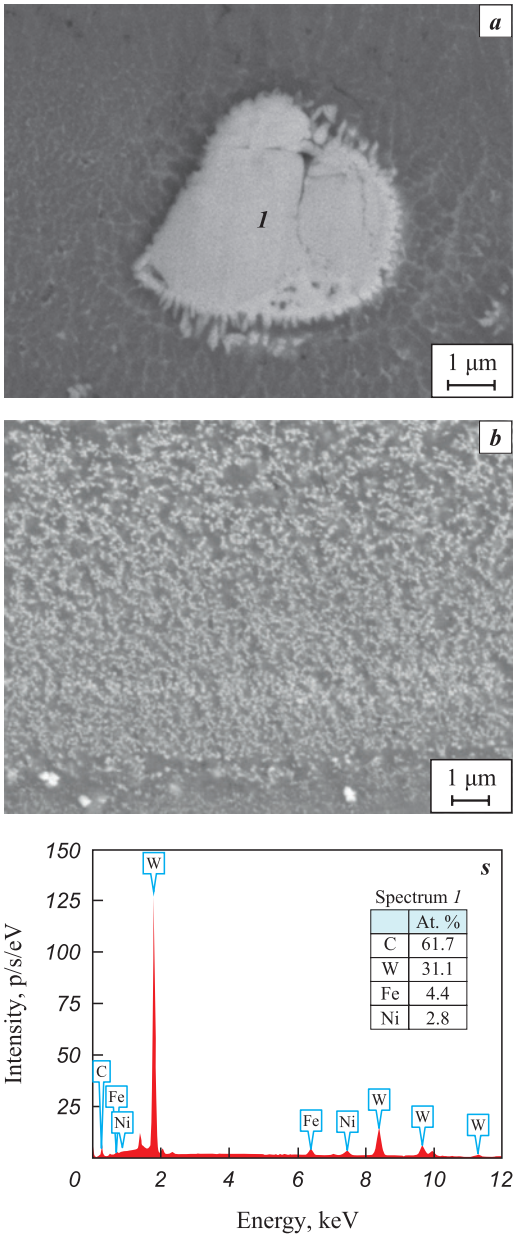


***Fig. 4.*** Microstructure images of the cross-section of ANW2 at magnifications of 25,000× (***a***) and 20,000× (***b***)

***c*** – EDS spectrum corresponding to Fig. 4, ***a***

***Рис. 4.*** Изображения микроструктуры поперечного сечения образца ANW2 при увеличениях 25 000× (***a***) и 20 000× (***b***)

***c*** – ЭДС-спектр к рис. 4, ***a***

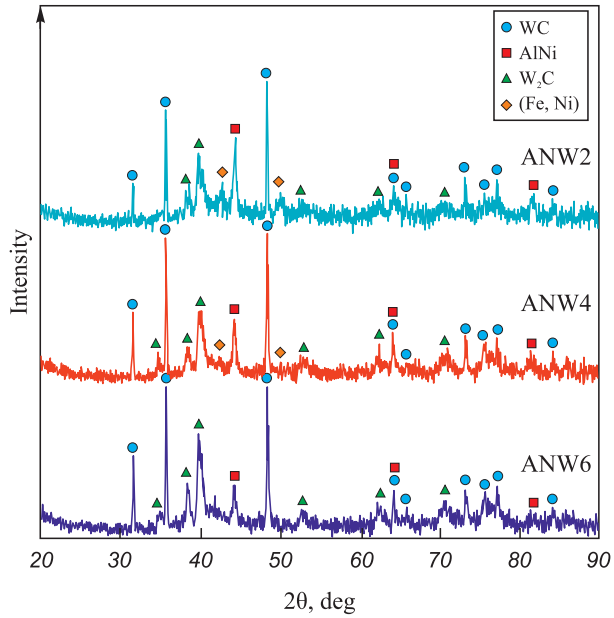


***Fig. 5.*** XRD patterns of the obtained coatings

***Рис. 5.*** Рентгеновские дифрактограммы полученных покрытий

the micro-melt pool on the substrate, ultimately forming the coating.

Microhardness measurements of WC/Ni–Al–Fe coatings revealed a monotonic increase in average values from 7.2 to 10.6 GPa as the tungsten carbide powder content in the NLE increased (Fig. 6). The microhardness of ANW2 and ANW4 samples remained similar (~7.5 GPa), which can be attributed to their structural similarity (see Figs. 3, *a–d*). Literature data indicate that the microhardness of plasma-clad $(NiAl)_{0.8}WC_{0.2}$–Fe(0–15 wt. %) coatings is significantly lower (4–6 GPa) due to their lower tungsten carbide content [17].

The results of tribological tests of WC/Ni–Al–Fe coatings are presented in Fig. 6. Depending on the WC concentration in the coatings, the friction coefficient varies non-monotonically from 0.61 to 0.73 under a 25 N load and from 0.62 to 0.70 under a 50 N load (Fig. 7, *a*). In both cases, the highest friction force values were observed for the ANW4 sample. The friction coefficient of the coatings was 8–31 % lower than that of 35 steel, demonstrating the anti-friction effect of tungsten carbide. Additionally, the amplitude of friction coefficient fluctuations for all coatings was significantly lower compared to 35 steel.

The specific wear rate of WC/Ni–Al–Fe coatings ranged from $(36–55)\cdot10^{-7}$ mm$^3$/(N·m) under a 25 N load and $(28–31)\cdot10^{-7}$ mm$^3$/(N·m) under a 50 N load, which is 11–24 times lower than that of 35 steel (Fig. 7, *b*). Unlike uncoated steel, the specific wear rate of the coatings at 50 N was lower than at 25 N. As the WC powder content in the NLE increased, the specific wear rate of the WC/Ni–Al–Fe coatings monotonically decreased under both loads. This trend aligns with Archard's wear theory, as it is attributed to the increase in coating hardness. Although the minimum specific wear rate was

***Table 3.* Semi-quantitative composition of the coatings**

***Таблица 3.* Полуколичественный состав покрытий**

| Sample | Phase, vol. % | | | |
|---|---|---|---|---|
| | WC | $W_2C$ | AlNi | FeNi |
| ANW2 | 48.6 | 14.1 | 28.2 | 9.0 |
| ANW4 | 61.5 | 14.9 | 18.7 | 4.9 |
| ANW6 | 65.5 | 24.1 | 10.3 | – |

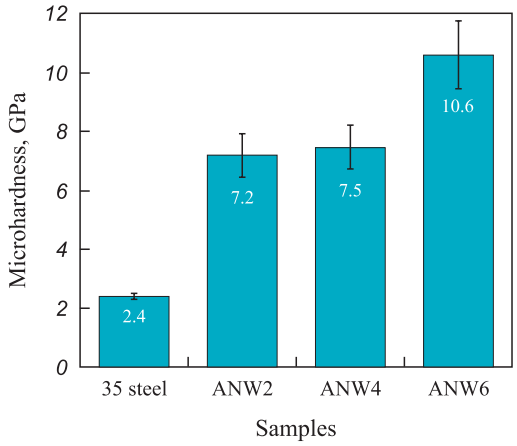


***Fig. 6.*** Average microhardness values of the coatings

***Рис. 6.*** Средние значения микротвердости покрытий

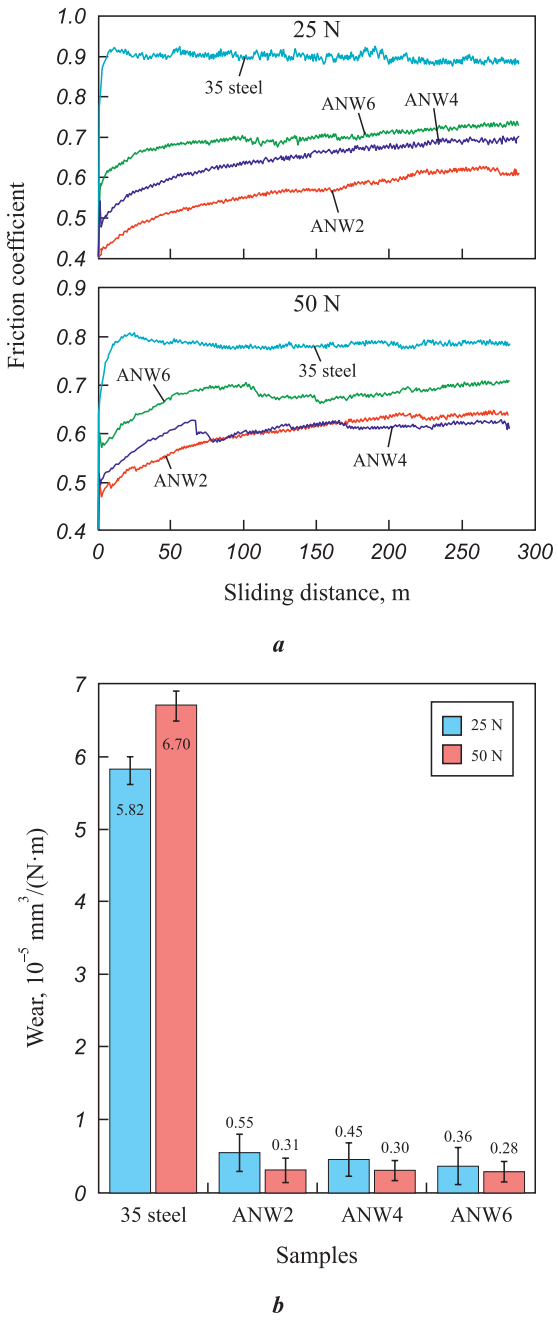


***Fig. 7.*** Coefficient of friction (***a***) and wear rate (***b***) of coatings compared to steel 35 at loads of 25 and 50 N

***Рис. 7.*** Коэффициент трения (***a***) и интенсивность изнашивания (***b***) исследуемых покрытий по сравнению со сталью 35 при нагрузках 25 и 50 Н

not observed within the tested compositions, further increasing the WC powder concentration in the NLE is impractical due to the reduction in cathode mass gain, iron enrichment of the coating matrix, and depletion of nickel and aluminum concentrations. The wear rate of plasma-clad $(NiAl)_{0.8}WC_{0.2}$–Fe(0–15 wt. %) coatings, as reported in [17], was significantly higher at $6.02 \cdot 10^{-5}$ mm$^3$/(N·m). This is likely due to their lower tungsten carbide concentration and lower hardness. Therefore, the proposed approach for producing Ni–Al–Fe coatings reinforced with tungsten carbide on steels appears to be more effective.

Electrochemical corrosion tests of WC/Ni–Al–Fe coatings were conducted in a 3.5 % NaCl solution using potentiodynamic polarization and impedance spectroscopy methods. Fig. 8, *a* presents Tafel polarization curves constructed from potentiodynamic experiments. The corrosion potential ($E_{corr}$) and corrosion current density ($I_{corr}$) were determined by extrapolating the cathodic and anodic slopes of the Tafel plots. As shown in Table 4, the corrosion potential of the coated samples ranged from –0.68 V to –0.57 V relative to the Ag/AgCl electrode. The highest $E_{corr}$ value was observed in the ANW4 sample, indicating its greater resistance to spontaneous corrosion compared to the other coatings. The corrosion current density of the coated samples ranged from $3.9 \cdot 10^{-5}$ to $2.5 \cdot 10^{-4}$ A/cm$^2$, with the lowest value recorded for ANW4 and the highest for ANW2. For uncoated 35 steel, the corrosion current density was $5.5 \cdot 10^{-5}$ A/cm$^2$. Given that corrosion rate is directly proportional to $I_{corr}$, it can be concluded that only the ANW4 coating improves the corrosion resistance of 35 steel by 29 %.

Fig. 8, *b* presents Bode impedance diagrams, which describe the frequency-dependent electrochemical behavior at the material-electrolyte interface. It is known that an increase in the impedance modulus (lg|*Z*|) at low frequencies hinders charge transfer, thereby improving the corrosion resistance of the material [32]. The WC/Ni–Al–Fe coatings can be ranked in ascending order of lg|*Z*| values as follows: ANW4, ANW2, and ANW6. Thus, the sample with the highest tungsten carbide concentration exhibits the greatest charge transfer resistance. According to the Bode plots, the impedance maximum of the steel substrate was higher than that of the coatings, indicating their weaker corrosion resistance. Notably, Ni–Al–Fe coatings without WC demonstrated higher charge transfer resistance [33]. This is likely due to the fact that conductive tungsten carbide disrupts the continuity of the $Al_2O_3$ barrier layer, which forms on the surface of WC/Ni–Al–Fe coatings in the electrolyte solution.

Overall, the corrosion resistance of WC/Ni–Al–Fe coatings can be considered weak, likely due to their relatively high iron concentration (35.5 to 57.6 at. %). Additionally, as a ceramic material with high electrical conductivity, tungsten carbide does not provide barrier protection against corrosion. Instead, it may form galvanic couples at the interface between the metallic matrix and WC particles.

***Table 4.* Corrosion potential and current density of WC/Ni–Al–Fe coatings in a 3.5 % NaCl solution**

***Таблица 4.* Потенциал и плотность тока коррозии WC/Ni–Al–Fe-покрытий в 3,5 %-ном растворе NaCl**

| Parameter | 35 steel | ANW2 | ANW4 | ANW6 |
|---|---|---|---|---|
| $E_{corr}$, V | –0.72 | –0.63 | –0.57 | –0.68 |
| $I_{corr}$, μA | 54.48 | 250.84 | 39.36 | 142.10 |

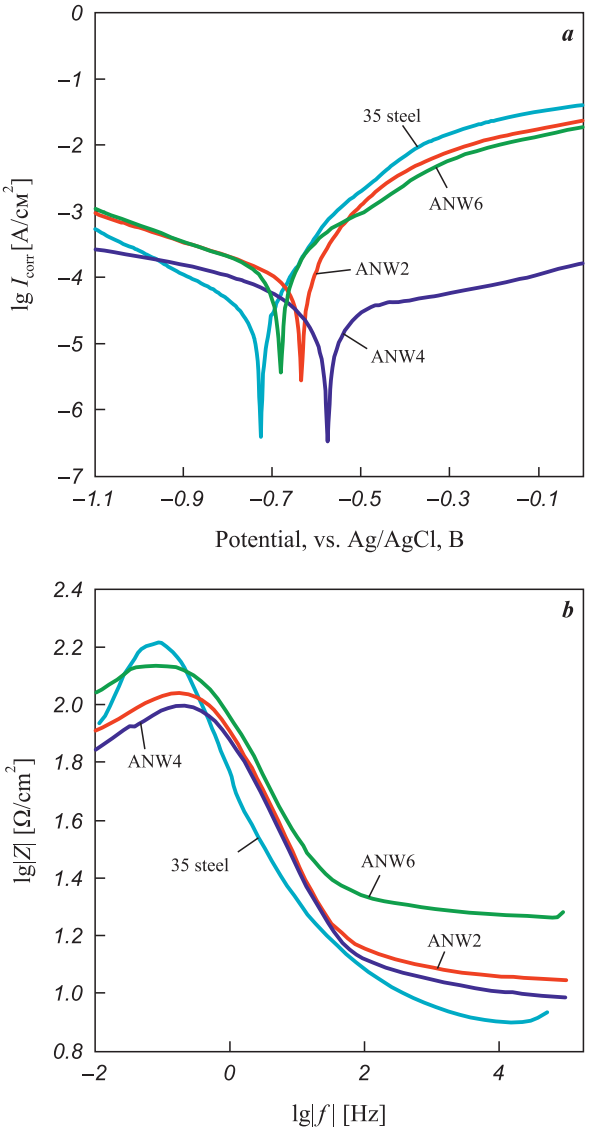


***Fig. 8.*** Polarization curves (***a***) and Bode impedance plots (***b***) of WC/Ni–Al–Fe coatings and 35 steel

***Рис. 8.*** Поляризационные кривые (***a***) и импедансные графики Боде (***b***) WC/Ni–Al–Fe-покрытий и стали 35

Fig. 9, *a* presents the results of cyclic oxidation resistance tests of 35 steel samples with WC/Ni–Al–Fe coatings at 700 °C. After 110 h of testing, the mass gain of the coated samples ranged from 8.3 to 39.8 g/m$^2$, while the steel substrate exhibited a significantly higher mass gain of 416.2 g/m$^2$. Thus, the application of WC/Ni–Al–Fe coatings enhances the oxidation resistance of 35 steel by a factor of 10.5 to 49.9. It should be noted that the mass gain of Ni–Al–Fe coatings produced without tungsten carbide under similar test conditions was comparable to the current results [33]. The oxidation resistance of the coated samples increased in the following order: ANW2, ANW6, and ANW4.

These findings indicate that incorporating up to 65 vol. % WC into the Ni–Al–Fe layer does not degrade its oxidation resistance. The ANW4 coating demonstrated the best performance, which aligns with the potentiodynamic polarization data (see Table 4). The mass gain during the oxidation resistance test resulted from the fixation of oxygen on the sample surfaces in the form of hematite ($Fe_2O_3$) and iron tungstate ($Fe_2WO_6$) (see Fig. 9, *b*), which forms through the simultaneous oxidation of iron and tungsten carbide:

$$WC + 2Fe + 4O_2 = Fe_2WO_6 + CO_2.$$

In addition to these compounds, $Fe_3W_3C$ and AlNi phases were also detected, further confirming the high oxidation resistance of the coatings. The $Fe_3W_3C$ phase forms due to the recrystallization of $W_2C$ during prolonged high-temperature exposure. Overall, all WC/Ni–Al–Fe coatings exhibited high oxidation resistance at 700 °C, comparable to that of metallic glasses [34], while also demonstrating greater wear resistance during wear testing.

## Conclusion

For the first time, metalloceramic WC/Ni–Al–Fe coatings were successfully deposited on 35 steel using the ESD method with a nonlocalized electrode, composed of nickel and aluminum granules (15 at. % Al and 85 at. % Ni) with 2, 4, and 6 vol. % WC powder. The coating matrix consisted of nickel aluminide (NiAl) and ferro-nickel, while α-WC and $W_2C$ inclusions acted as reinforcing phases. Increasing the WC powder content in the nonlocalized electrode led to a higher tungsten carbide concentration in the coatings.

Impedance and polarization experiments in a 3.5 % NaCl solution revealed that WC/Ni–Al–Fe coatings exhibit weak corrosion resistance, while their cyclic oxidation resistance at 700 °C was 10.5 to 49.9 times higher than that of 35 steel.

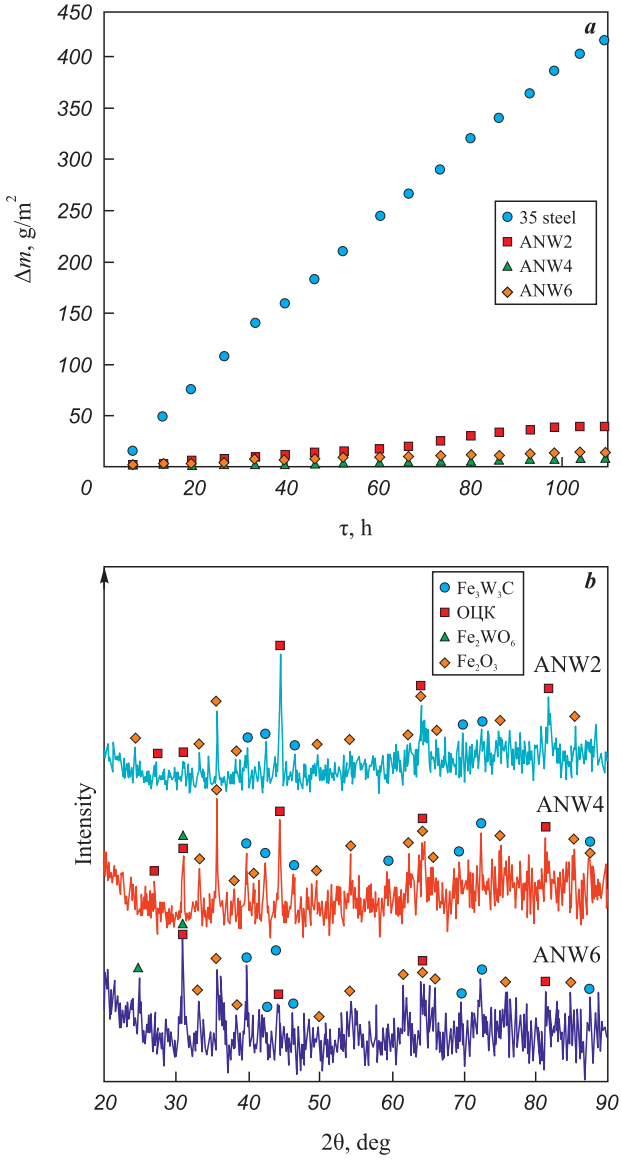


***Fig. 9.*** Cyclic oxidation resistance of coated samples at 700 °C (***a***) and XRD patterns of coatings after oxidation resistance testing (***b***)

***Рис. 9.*** Результаты циклических испытаний образцов на жаростойкость при температуре 700 °C (***a***) и рентгеновские дифрактограммы покрытий после этих испытаний (***b***)

Microhardness testing showed a monotonic increase from 7.2 to 10.6 GPa as the WC powder concentration in the nonlocalized electrode increased from 2 to 6 vol. %. The application of WC/Ni–Al–Fe coatings reduced the friction coefficient of 35 steel components by 8–31 % and lowered the specific wear rate by a factor of 11 to 24.

## References / Список литературы

1. Mari D., Bolognini S., Feusier G., Cutard T., Verdon C., Viatte T., Benoit W. TiMoCN based cermets: Part I. Morpho-

logy and phase composition. *International Journal of Refractory Metals and Hard Materials*. 2003;21(1–2):37–46. https://doi.org/10.1016/S0263-4368(03)00010-6

2. Wang L., Bai J., Wang Y., Men Z. A review of research progress on Ti (C, N)-based cermet binder by intermetallic compounds and high-entropy alloys. *Materials*. 2024;17(3):675. https://doi.org/10.3390/ma17030675
3. Erfanmanesh M., Abdollah-Pour H., Mohammadian-Semnani H., Shoja-Razavi R. Kinetics and oxidation behavior of laser clad WC–Co and Ni/WC–Co coatings. *Ceramics International*. 2018;44(11):12805–12814. https://doi.org/10.1016/j.ceramint.2018.04.087
4. Yang L.J., Wang S.P., Wang P., Li H., Yang H.Y., Ye Y.S., Li Z.X. Microstructural evolution and abrasive resistance of WC7Co ceramic particle-reinforced Ti6Al4V composite coating prepared by pulse laser cladding. *Journal of Iron and Steel Research International*. 2020;27(2):228–237. https://doi.org/10.1007/s42243-019-00359-y
5. Cheng J., Peng J., Wang M., Bo K., Li K., Zhang G., Yang Z. Effects of cyclic heating and water-cooling on the mechanical properties of WC–Co coatings. *Journal of Alloys and Compounds*. 2020;831:154769. https://doi.org/10.1016/j.jallcom.2020.154769
6. Dvornik M.I., Vlasova N.M. Comparative analysis of the tool life of submicron hard alloy WC-10Co sintered from powder obtained by electro discharge in oil. *Powder Metallurgy and Functional Coatings*. 2023;17(1):75–84. https://doi.org/10.17073/1997-308X-2023-1-75-84

   Дворник М.И., Власова Н.М. Сравнительный анализ эксплуатационной стойкости субмикронного твердого сплава WC–10Co, спеченного из порошка, полученного электроэрозионным диспергированием в масле. *Известия вузов. Порошковая металлургия и функциональные покрытия*. 2023;17(1):75–84. https://doi.org/10.17073/1997-308X-2023-1-75-84
7. Ojo-Kupoluyi O., Tahir S., Baharudin B., Azmah Hanim M., Anuar M. Mechanical properties of WC-based hardmetals bonded with iron alloys – A review. *Materials Science and Technology*. 2017;33:507–517. https://doi.org/10.1080/02670836.2016.1186929
8. Sun J., Zhao J., Gong F., Ni X., Li Z. Development and application of WC-based alloys bonded with alternative binder phase. *Critical Reviews in Solid State and Materials Sciences*. 2019;44(3):211–238. https://doi.org/10.1080/10408436.2018.1483320
9. Piechowiak D., Kania A., Łukaszkiewicz N., Miklaszewski A. Properties and microstructure evaluation in NiAl-*x*WC ($x$ = 0−90 wt. %) intermetallic-based composites prepared by mechanical alloying. *Materials*. 2023; 16(5):2048. https://doi.org/10.3390/ma16052048
10. Li X., Zhang M., Zheng D., Cao T., Chen J., Qu S. The oxidation behavior of the WC–10 wt.% $Ni_3Al$ composite fabricated by spark plasma sintering. *Journal of Alloys and Compounds*. 2015;629:148–154. https://doi.org/10.1016/j.jallcom.2015.01.010
11. Yao H.R., Bao Z.B., Shen M.L., Zhu, S.L., Wang F.H. A magnetron sputtered microcrystalline β-NiAl coating for SC superalloys. Part II. Effects of a NiCrO diffusion barrier on oxidation behavior at 1100 °C. *Applied Surface Science*. 2017;407:485–494. https://doi.org/10.1016/j.apsusc.2017.02.245
12. Deevi S.C. Advanced intermetallic iron aluminide coatings for high temperature applications. *Progress in Materials Science*. 2021;118:100769. https://doi.org/10.1016/j.pmatsci.2020.100769
13. Jia Q., Li D., Li S., Zhang Z., Zhang N. High-temperature oxidation resistance of NiAl intermetallic formed in situ by thermal spraying. *Coatings*. 2018;8(8):292. https://doi.org/10.3390/coatings8080292
14. Zou Y., Kusabiraki K., Saji S. Effect of Ni addition on formation of amorphous and nanocrystalline phase during mechanical alloying of Al–25 at.%Fe–(5,10) at.%Ni powders. *Materials research bulletin*. 2002;37(7):1307–1313. https://doi.org/10.1016/S0025-5408(02)00762-6
15. Schneibel J.H., George E.P., Specht E.D., Horton J.A. Strength, ductility, and fracture mode of ternary FeAl alloys. *MRS Online Proceedings Library*. 1994;364:73–78. https://doi.org/10.1557/PROC-364-73
16. Celik E., Culha O., Uyulgan B., Ak Azem N.F., Ozdemir I., Turk A. Assessment of microstructural and mechanical properties of HVOF sprayed WC-based cermet coatings for a roller cylinder. *Surface and Coatings Technology*. 2006;200(14–15):4320–4328. https://doi.org/10.1016/j.surfcoat.2005.02.158
17. Yuan J., Wang Q., Liu X., Lou S., Li Q., Wang Z. Microstructures and high-temperature wear behavior of NiAl/WC-$Fe_x$ coatings on carbon steel by plasma cladding. *Journal of Alloys and Compounds*. 2020;842:155850. https://doi.org/10.1016/j.jallcom.2020.155850
18. Xu B., Zhu Z., Ma S., Zhang W., Liu W. Sliding wear behavior of Fe–Al and Fe–Al/WC coatings prepared by high velocity arc spraying. *Wear*. 2004;257(11):1089–1095. https://doi.org/10.1016/j.wear.2004.05.012
19. Mostajeran A., Shoja-Razavi R., Hadi M., Erfanmanesh M., Barekat M., Firouzabadi M.S. Evaluation of the mechanical properties of WC–FeAl composite coating fabricated by laser cladding method. *International Journal of Refractory Metals and Hard Materials*. 2020;88:105199. https://doi.org/10.1016/j.ijrmhm.2020.105199
20. Zhou J., Huang Y., Liang G., Zhao J., Hao X. Effect of copper on microstructure and performance of WC/NiAl/TiC composite coatings by laser cladding. *Advanced Engineering Materials*. 2024;26(10):2302059. https://doi.org/10.1002/adem.202302059
21. Jamnapara N.I., Frangini S., Alphonsa J., Chauhan N.L., Mukherjee S. Comparative analysis of insulating properties of plasma and thermally grown alumina films on electrospark aluminide coated 9Cr steels. *Surface and Coatings Technology*. 2015;266:146–150. https://doi.org/10.1016/j.surfcoat.2015.02.028
22. Burkov A.A., Kulik M.A. Electrospark deposition and structure of ceramic-metal WC/Fe–Al coatings. *Svarochnoye proizvodstvo*. 2023;2:26–32. (In Russ.). https://doi.org/10.34641/SP.2023.1059.2.013

    Бурков А.А., Кулик М.А. Электроискровое осаждение и структура металлокерамических WC/Fe–Al покрытий. *Сварочное производство*. 2023;2:26–32. https://doi.org/10.34641/SP.2023.1059.2.013

**23.** Burkov A.A. Wear resistance of electrospark WC–Co coatings with different iron contents. *Journal of Friction and Wear*. 2016;37(4):385–388. https://doi.org/10.3103/s1068366616040048

**24.** Verkhoturov A.D. Formation of the surface layer of metals during electrospark deposition. Vladivostok: Dal'nauka, 1995. 323 p. (In Russ.).

Верхотуров А.Д. Формирование поверхностного слоя металлов при электроискровом легировании. Владивосток: Дальнаука, 1995. 323 с.

**25.** Kwok D.Y., Neumann A.W. Contact angle measurement and contact angle interpretation. *Advances in Colloid and Interface Science*. 1999;81(3):167–249. https://doi.org/10.1016/S0001-8686(98)00087-6

**26.** Burkov A.A., Krutikova V.O., Bytsura A.Yu., Khe V.K. Ti–Cr–Cu electrospark coatings on steel St3. *Problemy chernoi metallurgii i materialovedeniya*. 2023;(1): 93–104. (In Russ.). https://doi.org/10.54826/19979258_2023_1_93

Бурков А.А., Крутикова В.О., Быцура А.Ю., Хе В.К. Ti–Cr–Cu электроискровые покрытия на стали Ст3. *Проблемы черной металлургии и материаловедения*. 2023;(1):93–104. https://doi.org/10.54826/19979258_2023_1_93

**27.** Burkov A.A., Chigrin P.G., Kulik M.A. The influence of the working conditions of the electrospark granules deposition on the formation of cracks in Ti–Al intermetallic coatings. *Solid State Phenomena*. 2021;316:814–820. https://doi.org/10.4028/www.scientific.net/SSP.316.814

**28.** Burkov A.A., Pyachin S.A. Investigation of WC–Co electrospark coatings with various carbon contents. *Journal of Materials Engineering and Performance*. 2014;23(6):2034–2042. https://doi.org/10.1007/s11665-014-0974-z

**29.** Nurminen J., Näkki J., Vuoristo P. Microstructure and properties of hard and wear resistant MMC coatings deposited by laser cladding. *International Journal of Refractory Metals and Hard Materials*. 2009;27(2):472–478. https://doi.org/10.1016/J.IJRMHM.2008.10.008

**30.** Jin H., Ji R., Dong T., Liu S., Zhang F., Zhao L., Liu Y. Efficient fabrication and characterization of Ni–Fe–WC composite coatings with high corrosion resistance. *Journal of Materials Research and Technology*. 2022;16:152–167. https://doi.org/10.1016/j.jmrt.2021.11.145

**31.** Kayali Y., Talaş Ş. Investigation of wear and corrosion behaviour of AISI 316 L stainless steel coated by ESD surface modification. *Protection of Metals and Physical Chemistry of Surfaces*. 2019;55(6):1148–1153. https://doi.org/10.1134/S2070205119060170

**32.** Rosalbino F., Scavino G. Corrosion behaviour assessment of cast and HIPed Stellite 6 alloy in a chloride-containing environment. *Electrochimica Acta*. 2013;111:656–662. https://doi.org/10.1016/j.electacta.2013.08.019

**33.** Burkov A.A., Kulik M.A., Bytsura A.Yu. Structure and properties of Al–Ni–Fe coatings on Steel 35 obtained by electrospark deposition. *Metal Science and Heat Treatment*. 2024;66(7):415–422. https://doi.org/10.1007/s11041-024-01065-7

Бурков А.А., Кулик М.А., Быцура А.Ю. Структура и свойства Al–Ni–Fe-покрытий на стали 35, полученных методом электроискрового легирования. *Металловедение и термическая обработка металлов*. 2024;7: 22–30. https://doi.org/10.30906/mitom.2024.7.22-30

**34.** Lee C.Y., Sheu H.H., Tsay L.W., Hsiao P.S., Lin T.J., Lee H.B. The effect of heat treatment on the corrosion resistance of Fe-based amorphous alloy coating prepared by high velocity oxygen fuel method. *Materials*. 2021; 14(24):7818. https://doi.org/10.3390/ma14247818

## Information about the Author

***Aleksandr A. Burkov*** – Cand. Sci. (Phys.-Math.), Senior Researcher, Head of the Laboratory of Physical and Chemical Fundamentals of Materials Technology, Institute of Materials Science of the Khabarovsk Federal Research Center of the Far Eastern Branch of the Russian Academy of Sciences
***ORCID***: 0000-0002-5636-4669
***E-mail:*** burkovalex@mail.ru

## Сведения об авторе

***Александр Анатольевич Бурков*** – к.ф.-м.н., ст. науч. сотрудник, зав. лабораторией физико-химических основ технологии материалов, Институт материаловедения Хабаровского федерального исследовательского центра Дальневосточного отделения РАН
***ORCID***: 0000-0002-5636-4669
***E-mail:*** burkovalex@mail.ru

Received 19.08.2024
Revised 21.01.2025
Accepted 24.01.2025

Статья поступила 19.08.2024 г.
Доработана 21.01.2025 г.
Принята к публикации 24.01.2025 г.